Journal of Coordination Chemistry
Publication details, including instructions for authors and subscription information:
http://www.tandfonline.com/loi/gcoo20

Synthesis and characterization of a coplanar-shaped hexa-Cu^{II} sandwiched arsenotungstate

Jiai Hua [a b], Suzhi Li [a b], Xiang Ma [a b], Pengtao Ma [a b], Jingping Wang [a b] & Jingyang Niu [a b]

[a] Institute of Molecular and Crystal Engineering, College of Chemistry and Chemical Engineering, Henan University, Kaifeng 475004, P.R. China

[b] Basic Experimental Teaching Center, Henan University, Kaifeng 475004, P.R. China

Published online: 23 Apr 2012.

To cite this article: Jiai Hua, Suzhi Li, Xiang Ma, Pengtao Ma, Jingping Wang & Jingyang Niu (2012) Synthesis and characterization of a coplanar-shaped hexa-Cu^{II} sandwiched arsenotungstate, Journal of Coordination Chemistry, 65:10, 1740-1749, DOI: 10.1080/00958972.2012.680210

To link to this article: http://dx.doi.org/10.1080/00958972.2012.680210

Journal of Coordination Chemistry
Vol. 65, No. 10, 20 May 2012, 1740–1749

Synthesis and characterization of a coplanar-shaped hexa-Cu^{II} sandwiched arsenotungstate

JIAI HUA†‡, SUZHI LI†‡, XIANG MA†‡, PENGTAO MA†‡, JINGPING WANG†‡* and JINGYANG NIU†‡*

†Institute of Molecular and Crystal Engineering, College of Chemistry and Chemical Engineering, Henan University, Kaifeng 475004, P.R. China
‡Basic Experimental Teaching Center, Henan University, Kaifeng 475004, P.R. China

(*Received 19 December 2011; in final form 28 February 2012*)

An organic–inorganic coplanar-shaped hexa-Cu^{II} sandwiched hybrid, $(H_2en)\{[Cu(en)_2]_2[Cu_2(en)_2Cu_4(H_2O)_2](B\text{-}\alpha\text{-}AsW_9O_{34})_2\} \cdot 5H_2O$ (en = ethylenediamine) (**1**), has been synthesized *via* hydrothermal method and further characterized by IR spectroscopy, thermogravimetric analysis, and X-ray single-crystal diffraction. Single-crystal X-ray diffraction analysis shows that **1** contains an organic–inorganic hybrid polyoxoanion $\{Cu_2(en)_2Cu_4(H_2O)_2(B\text{-}\alpha\text{-}AsW_9O_{34})_2\}^{6-}$, which can be described as a coplanar-shaped hexa-Cu^{II} cluster sandwiched by two trivacant $[B\text{-}\alpha\text{-}AsW_9O_{34}]^{9-}$ fragments. Complex **1** represents a rare organic–inorganic coplanar-shaped hexa-Cu^{II} cluster sandwiched arsenotungstate. Magnetic susceptibility measurements indicate that **1** demonstrates ferromagnetic coupling interactions within the Cu^{II} centers.

Keywords: Polyoxometalates; Arsenotungstate; Sandwich-type; Coplanar-shaped hexa-Cu^{II}

1. Introduction

Polyoxometalates (POMs), a large and distinct class of metal-oxygen clusters, with various compositions, fascinating structures, and remarkable physicochemical properties, have received substantial attention because of potential applications in catalysis, materials science, medicine, and electrochemistry [1–5]. As one subfamily of POMs, transition-metal-substituted polyoxometalates (TMSPs) exhibit promising catalytic properties due to the incorporation of TMs with POMs [6, 7]. Within this class, sandwich-type TMSPs represent an important domain and high-nuclearity transition-metal (TM) clusters have attracted interest in solid-state materials chemistry because of applications in photochemistry, catalysis, and magnetism [8–16]. Among the sandwich-type POMs, pure inorganic di- to penta-TM substituted POMs predominate, $[\{SiM_2W_9O_{34}(H_2O)\}_2]^{12-}$ $(M = Mn^{II}/Cu^{II}/Zn^{II})$ [17], $[(\alpha\text{-}XW_9O_{33})_2M_3(H_2O)_3]^{n-}$ $(M = Cu^{II}/Zn^{II}/Mn^{II}/Co^{II}$; $X = As^{III}/Sb^{III}/Se^{IV}/Te^{IV})$ [18, 19], $[Fe_4(H_2O)_{10}(\beta\text{-}XW_9O_{33})_2]^{n-}$ $(X = As^{III}/Sb^{III}/Se^{IV}/Te^{IV})$ [20], $[(n\text{-}C_4H_9)_4N]_{11}H_5[Cu_4(P_2W_{15}O_{56})_2]$ [21], and $[Cu_5(OH)_4(H_2O)_2(A\text{-}\alpha\text{-}SiW_9O_{33})_2]^{10-}$ [22] as well as

*Corresponding authors. Email: jpwang@henu.edu.cn; jyniu@henu.edu.cn

ISSN 0095-8972 print/ISSN 1029-0389 online
http://dx.doi.org/10.1080/00958972.2012.680210

$K_3H_4Cu_{0.5}\{Cu[Cu_{7.5}Si_2W_{16}O_{60}(H_2O)_4(OH)_4]_2\} \cdot 9H_2O$ [23]. Compared with inorganic sandwich-type TMSPs, investigations of hexa-TM substituted sandwich-type POMs remain largely unexplored. Since Kortz *et al.* reported the first hexa-Fe^{III} sandwiched germanotungstate $[Fe_6(OH)_3(A\text{-}\alpha\text{-}GeW_9O_{34}(OH)_3)_2]^{11-}$ in 2005 [24], several hexa-TM sandwiched POMs have been obtained, such as $[(CuCl)_6(AsW_9O_{33})_2]^{12-}$, $[(MnCl)_6(SbW_9O_{33})_2]^{12-}$ [25], $[\{Ni_6(H_2O)_4(\mu_2\text{-}H_2O)_4(\mu_3\text{-}OH)_2\}(\alpha\text{-}SiW_9O_{34})_2]^{10-}$ [26], and $[Cu(enMe)_2]_2\{[Cu(enMe)_2(H_2O)]_2[Cu_6(enMe)_2(B\text{-}\alpha\text{-}SiW_9O_{34})_2]\} \cdot 4H_2O$ [27]. In 2008, our group also synthesized two hexa-TM sandwiched POMs, $[Cu(2,2'\text{-bipy})]_2[Cu(2,2'\text{-bipy})_2]_2[Cu_6(2,2'\text{-bipy})_2(GeW_9O_{34})_2] \cdot 3H_2O$, and $(Cuphen)_2[Cu(phen)_2]_2[Cu_6phen_2(GeW_9O_{34})_2] \cdot 2H_2O$ [28]. Obviously the highest nuclear TM-sandwiched POMs are mainly constructed by $[GeW_9O_{34}]^{10-}$ or $[SiW_9O_{34}]^{10-}$ building blocks; reports on arsenotungstates (ATs) are limited although ATs are an important subfamily possessing enormous diversity of properties and structures in POM chemistry. Previously reported hexa-nuclear ATs are purely inorganic and synthesized by a conventional aqueous solution method, which provides a good opportunity to exploit the {As–O–W} system simultaneously containing organic and inorganic components under hydrothermal conditions. To obtain organic–inorganic hybrid high-nuclear ATs, we investigate the hydrothermal behavior of the {As–O–W} system with organic components. Even small amounts of organic components can influence the structures of the resulting products. By making full use of ethylenediamine (en), recently we synthesized an organic–inorganic hybrid hexa-nuclear Zn substituted AT $[Zn(Hen)]_6[B\text{-}\alpha\text{-}AsW_9O_{33}]_2 \cdot 6H_2O$ [29]. As a continuation of our work, herein, we report a hexa-Cu^{II} cluster sandwiched hybrid $(H_2en)\{[Cu(en)_2]_2[Cu_2(en)_2Cu_4(H_2O)_2](B\text{-}\alpha AsW_9O_{34})_2\} \cdot 5H_2O$ (en = ethylenediamine) (**1**), which represents a rare coplanar-shaped hexa-Cu^{II} substituted sandwich-type organic–inorganic AT.

2. Experimental

$Na_9[\alpha\text{-}AsW_9O_{33}] \cdot 19H_2O$ was prepared according to the literature [30] and confirmed by infrared (IR) spectra. All other chemicals used for synthesis were of reagent grade and used without purification.

2.1. *Preparation of $(H_2en)\{[Cu_2(en)_2]_2[Cu_2(en)_2\ Cu_4(H_2O)_2](B\text{-}\alpha\text{-}AsW_9O_{34})_2\} \cdot 5H_2O$*

A mixture of $Na_9[\alpha\text{-}AsW_9O_{33}] \cdot 19H_2O$ (0.111 g, 0.0397 mmol), $Cu(NO_3)_2 \cdot 2H_2O$ (0.096 g, 0.397 mmol), en (0.036 mL, 0.538 mmol), C_2H_5OH (0.036 mL, 0.538 mmol), DMF (0.017 mL, 0.221 mmol), and 12 mL H_2O was stirred for an hour in air. The pH of the mixture was adjusted to 3.4–3.9 with 4 mol L^{-1} HCl, and then the mixture was sealed in a 20 mL Teflon-lined stainless steel autoclave and heated at 150°C for 3 days under autogenous pressure. After slowly cooling to ambient temperature, purple crystals were isolated, washed with distilled water, and dried at ambient temperature (14% yield based on $Na_9[\alpha\text{-}AsW_9O_{33}] \cdot 19H_2O$).

2.2. *Physical measurements*

IR spectra were obtained from KBr pellets on a Nicolet 170 SXFT-IR spectrophotometer from 4000 cm^{-1} to 400 cm^{-1}. Thermogravimetric (TG) analyses were conducted on a Mettler-Toledo TGA/SDTA 851[e] thermal analyzer in flowing air with a heating rate of 10°C min^{-1} from 25°C to 800°C. Magnetic susceptibility measurements were obtained with a Quantum Design MPMS-XL7 SQUID magnetometer from 2 K to 300 K.

2.3. *X-ray crystallography*

Intensity data of **1** were collected on a Bruker Apex-2 CCD detector using graphite monochromated Mo-Kα radiation (λ = 0.71073 Å) at 296 K. Both structures were solved by direct methods and refined using full-matrix least-squares on F^2. The remaining atoms were found from successive full-matrix least-squares refinements on F^2 and Fourier syntheses. All calculations were performed using the SHELXL-97 program package [31]. Intensity data were corrected for Lorentz and polarization effects as well as for multi-scan absorption. No hydrogen atoms associated with water were located from the difference Fourier map. Positions of hydrogen atoms attached to carbon and nitrogen were geometrically placed. All hydrogen atoms were refined isotropically as a riding mode using the default SHELXTL parameters. A summary of crystal data and structure refinements for **1** is listed in table 1.

Table 1. Crystallographic data and structural refinements for **1**.

	1
Empirical formula	$C_{14}H_{72}As_2Cu_8N_{14}O_{75}W_{18}$
Formula weight	5604.32
Temperature (K)	296(2)
Crystal system	Monoclinic
Space group	$P2(1)/c$
Unit cell dimensions (Å, °)	
a	11.8365(19)
b	33.122(5)
c	12.232(2)
β	108.931(3)
Volume (Å^3), Z	4536.3(13), 2
Calculated density (g cm^{-3})	4.103
Absorption coefficient (mm^{-1})	25.377
F(000)	4968
Crystal size (mm^3)	0.48 × 0.16 × 0.04
θ range for data collection (°)	1.82–25.00
Limiting indices	$-14 \le h \le 12$; $-39 \le k \le 26$; $-14 \le l \le 14$
Reflections collected	22,772
Independent reflection	7965 [R(int) = 0.0585]
Refinement method	Full-matrix least-squares on F^2
Goodness-of-fit on F^2	1.032
Final R indices [$I > 2\sigma(I)$]	$R_1 = 0.0491$, $wR_2 = 0.1134$

3. Results and discussion

3.1. *Synthesis*

Compound **1** was synthesized from $[\alpha\text{-}AsW_9O_{33}]^{9-}$, but the product contains $[\alpha\text{-}AsW_9O_{34}]^{9-}$, indicating that during the reaction oxidization of $[\alpha\text{-}AsW_9O_{33}]^{9-} \rightarrow [\alpha\text{-}AsW_9O_{34}]^{9-}$ occurred when the system temperature was heated to 150°C. However, when we used $Na_2WO_4 \cdot 2H_2O$ and $NaAsO_2$ to replace $[B\text{-}\alpha\text{-}AsW_9O_{33}]^{9-}$ in the presence of $Cu(NO_3)_2 \cdot 2H_2O$ and en under similar conditions to **1**, we failed to obtain **1**. Compared with $[H_2dap]_6H_8[Ni_4(H_2O)_2(B\text{-}\alpha AsW_9O_{34})_2]_2 \cdot 33H_2O$ or $\{[Ni(dap)_2(H_2O)]_2[Ni(dap)_2]_2[Ni_4(Hdap)_2(B\text{-}\alpha\text{-}AsW_9O_{34})_2]\} \cdot 4H_2O$ [32] and $[Ni(en)_2]_2[\{Ni_3(en)_6(H_2O)_2Ni_4(H_2O)_2(\alpha\text{-}PW_9O_{34})_2\}] \cdot 7H_2O$ which were synthesized with $Na_8[A\text{-}\alpha\text{-}HAsW_9O_{34}] \cdot 11H_2O$ or $Na_9[\alpha\text{-}PW_9O_{34}] \cdot 16H_2O$ [15] and TMs as reactants, where we only obtain tetra-TM substituted sandwich-type POMs, oxidization of $[\alpha\text{-}AsW_9O_{33}]^{9-}$ may promote formation of the high-nuclear TM cluster [29]. Appropriate pH is the key factor. To investigate the effect of pH on the final products, a series of parallel experiments were carried out; **1** was obtained in the pH range of 3.4–3.9. When the pH was beyond this range, only amorphous powers were obtained, indicating that pH plays an important role in isolation and crystallization of **1**. When Cu^{2+} was replaced by Ni^{2+} or Co^{2+}, we also got amorphous powers. It is obvious that many factors such as temperature, As-containing materials, pH and TM influence the type of building blocks and the amount of TM incorporated into the core of the sandwich-type compounds. Therefore, further investigation is in progress.

3.2. *Crystal structures of 1*

The single-crystal X-ray diffraction analysis reveals that **1** crystallizes in the monoclinic space group $P2(1)/c$ and its molecular structure unit contains one Cu_6-substituted sandwich-type polyoxoanion $\{Cu_2(en)_2Cu_4(H_2O)_2(B\text{-}\alpha\text{-}AsW_9O_{34})_2\}^{6-}$ (figure 1a), one isolated $(H_2en)^{2+}$ as counter ion, two pendant $[Cu(en)_2]^{2+}$ cations, and five crystallization water molecules. The Cu_6-substituted sandwich-type polyoxoanion $\{Cu_2(en)_2Cu_4(H_2O)_2(B\text{-}\alpha\text{-}AsW_9O_{34})_2\}^{6-}$ is constructed from a coplanar hexa-Cu^{II} $\{Cu_2(en)_2Cu_4(H_2O)_2\}$ ($\{Cu_6\}$) cluster (figure 1b) sandwiched by two trivacant Keggin $[B\text{-}\alpha\text{-}AsW_9O_{34}]^{9-}$ units (figure 1c) (formed by removing three edge-sharing WO_6 octahedra belonging to one edge-sharing W_3O_{13} triad from saturated Keggin structure) in a staggered configuration, resulting in a rare bi-TM-supported sandwich-type structure with idealized C_i symmetry. There are three kinds of oxygen atoms in the trivacant Keggin $[B\text{-}\alpha\text{-}AsW_9O_{34}]^{9-}$ subunit: W–O_t (terminal) 1.693(11)–1.719(11) Å, W–$O_{b,c}$ (bridge) 1.772(11)–2.063(11) Å, W–O_a (central) 2.334(10)–2.371(11) Å, and As–O 1.658(9)–1.693(11) Å. The hexa-Cu^{II} $\{Cu_2(en)_2Cu_4(H_2O)_2\}$ cluster in **1** represents a rare hexa-Cu^{II} cluster sandwiched by two $[B\text{-}\alpha\text{-}AsW_9O_{34}]^{9-}$ fragments *via* 14 bridging oxygen atoms from lacunae of two $[B\text{-}\alpha\text{-}AsW_9O_{34}]^{9-}$ units, two μ_4-O from two AsO_4 tetrahedra and 12 μ_2-O from 12 WO_6 octahedra. In the central $\{Cu_6\}$ cluster of **1**, Cu1, Cu2, and Cu3 form a $\{Cu_6\}$ cluster by the structure-directing role of lacunary sites of two $[B\text{-}\alpha\text{-}AsW_9O_{34}]^{9-}$ units, six Cu^{2+} exhibit three kinds of coordination environments. Both Cu1 and Cu2 form two distorted octahedral coordination configurations (Cu–O_{POM}: 1.973(10)–2.210(9) Å, Cu–O_W: 2.091(11) Å), which are just located at the four vacant sites of two $[B\text{-}\alpha\text{-}AsW_9O_{34}]^{9-}$ moieties to form a sandwich

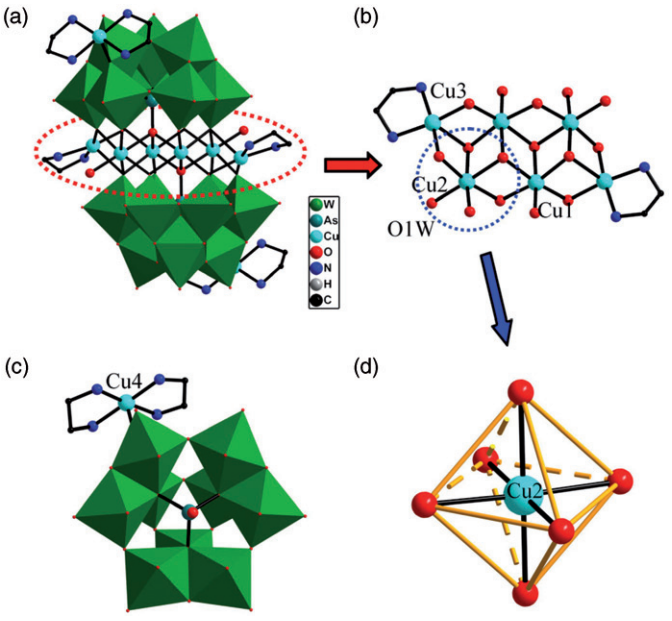

Figure 1. (a) Combined polyhedral/ball-and-stick representation of **1**. Lattice molecules are omitted for clarity. (b) Ball-and-stick view of $\{Cu_2(en)_2Cu_4(H_2O)_2\}^{12+}$. (c) Polyhedral view of the $[B\text{-}\alpha\text{-}AsW_9O_{34}]^{9-}$ fragment. (d) The coordination environment around Cu2. Color code: WO_6 octahedra: green; As: teal; Cu: turquoise; N: blue; O: red; C: black.

$[Cu_4(B\text{-}\alpha\text{-}AsW_9O_{34})_2]^{12-}$ fragment. The independent Cu1 and Cu2 ions exhibit different coordination environments. Cu1 is coordinated by six oxygen atoms from two $[B\text{-}\alpha\text{-}AsW_9O_{34}]^{9-}$ fragments, whereas Cu2 is defined by five oxygen atoms from two $[B\text{-}\alpha\text{-}AsW_9O_{34}]^{9-}$ units and one H_2O (figure 1d), different from previously reported hexa-TM clusters [27]. Cu3 adopts a distorted square-pyramidal geometry defined by two nitrogen atoms from an en (Cu–N: 1.963(15)–2.013(14)) Å) and three oxygen atoms (Cu–O_{POM}: 1.947(10)–2.421(11) Å) from two $[B\text{-}\alpha\text{-}AsW_9O_{34}]^{9-}$ units. In the skeleton of **1**, as a result of Jahn–Teller distortion, the five-coordinate Cu4 adopts a distorted square-pyramidal geometry, with four nitrogen atoms from two en [Cu–N: 1.971(17)–2.015(16) Å] and one bridging oxygen [Cu–O: 2.641 Å] from the POM backbone situated on the basal plane.

Only four kinds of organic–inorganic hybrid hexa-TM cluster sandwiched POMs have been reported. As shown in figure 2, although the coplanar hexa-Cu^{II} cluster (figure 2a) in **1** is similar to the reported hexa-Cu^{II} $\{[Cu(enMe)]_2Cu_4O_{14}\}$ cluster in $[Cu(enMe)_2]_2\{[Cu(enMe)_2(H_2O)]_2[Cu_6(enMe)_2(B\text{-}\alpha\text{-}SiW_9O_{34})_2]\}\cdot 4H_2O$ [27] (figure 2b), two essential differences are observed: (a) the hexa-Cu^{II} cluster in **1** contains four CuO_6 octahedra and two CuO_3N_2 square pyramids *via* edge-sharing mode. However, the hexa-Cu^{II} $\{[Cu(enMe)]_2Cu_4O_{14}\}$ cluster is constructed from two CuO_6 octahedra, two CuO_5, and two CuO_3N_2 square pyramids; (b) the POM backbone in **1** is AT, whereas the latter is silicotungstate. This hexa-Cu^{II} cluster in **1** represents a rare organic–inorganic hybrid ATs in the family of sandwich-type TMSPs. Very recently, our lab reported a hexa-Cu^{II} $[Cu_4(H_2O)_4Cu_2(phen)_2]^{12+}$ cluster sandwiched AT $[Cu_2(phen)_2(\mu ox)]\{[Cu(phen)(H_2O)_2][Cu_4(H_2O)_4Cu_2(phen)_2(AsW_9O_{33})_2]\}\cdot 6H_2O$ [33], which

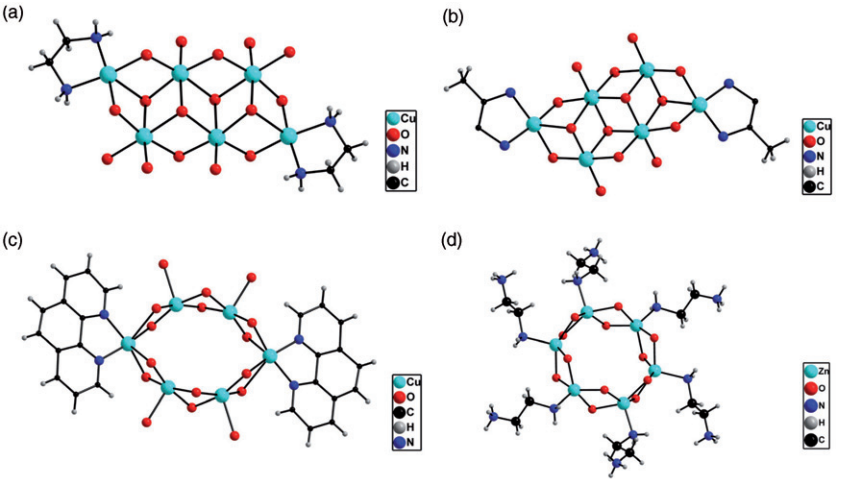

Figure 2. Comparison of ball-and-stick illustrations of some representative inorganic–organic hybrid hexa-TM clusters.

exhibits a hexa-Cu^{II} cluster (figure 2c): the alternate arrangement of two five-coordinate Cu^{2+} ions and a six-coordinate Cu^{2+} forms a coplanar six-member ring. In 2011, the organic–inorganic hexa-nuclear Zn substituted AT $[Zn(Hen)]_6[B\text{-}\alpha\text{-}AsW_9O_{33}]_2 \cdot 6H_2O$ [29] was reported by us, in which the hexa-Zn cluster in the sandwich displays a turbine-shaped alignment with end-on coordination of en (figure 2d).

3.3. *IR spectrum*

The IR spectrum of **1** (Supplementary material) shows similar asymmetric vibrations to other $[B\text{-}\alpha\text{-}AsW_9O_{34}]^{9-}$-containing species [34]. In the low-wavenumber region, four characteristic bands assigned to the $\nu(W\text{–}O_t)$, $\nu(As\text{–}O_a)$, $\nu(W\text{–}O_b)$, and $\nu(W\text{–}O_c)$ appear at 953, 879, 857, and 737 cm^{-1}, respectively, indicating the presence of polyoxoanions. In addition, characteristic bands at 3151–3317 cm^{-1} are ascribed to stretching vibrations of N–H which confirms the presence of en. Vibration at 3493 cm^{-1} can be assigned to –OH stretch. The IR spectrum is in good agreement with the result of X-ray diffraction structural analysis.

3.4. *TG analysis*

The TG curve of **1** (Supplementary material) exhibits two steps of weight loss from 25°C to 600°C. The first step occurs from 25°C to 125°C, corresponding to loss of five crystallization water molecules (1.65%) in agreement with the calculated value (1.60%). The second weight loss of 12.21% from 125°C to 490°C can be assigned to loss of seven en ligands, two coordination water molecules, partial As_2O_3, and oxygen from decomposition of two $[B\text{-}\alpha\text{-}AsW_9O_{34}]^{9-}$ fragments (Calcd 12.44%) [35, 36]. The whole weight loss (13.86%) is consistent with the calculated value (14.04%).

3.5. *Magnetic property*

The nonmagnetic polyoxoanion framework not only guarantees effective magnetic isolation of the TM cluster, providing good opportunity to investigate magnetic exchange interactions and electron delocalization, but can also control the magnitude of magnetic couplings [37, 38]. Since **1** incorporates hexa-Cu^{II} cluster sandwiched by nonmagnetic fragments, it is exciting to probe its magnetic properties, thus, the solid state direct-current magnetic susceptibility of **1** has been measured on polycrystalline samples from 2 K to 300 K. The magnetic data for **1** are plotted in figure 3 as χ_M and $\chi_M T$ *versus* T. The temperature dependence of χ_M shows a slight increase from 0.010 to 0.099 emu mol^{-1} from 300 K to 40 K and then exponentially reaches the maximum value of 1.729 emu mol^{-1} at 2 K. Correspondingly, the $\chi_M T$ of 2.93 emu K mol^{-1} at 300 K is consistent with the theoretical value (3.00 emu K mol^{-1}) expected for eight noninteracting Cu^{II} cations ($S = 1/2$) in **1** supposing $g = 2$. Upon cooling, the value of $\chi_M T$ increases to the maximum value of 4.549 emu K mol^{-1} at 7 K. Further decrease in the temperature results in a decrease in the $\chi_M T$ product, which takes the value of 4.478 emu K mol^{-1} at 2 K. This behavior agrees with the presence of dominant ferromagnetic exchange interactions within the belt-like hexa-Cu^{II} clusters mediated by the oxygen bridges. The dependence of the reciprocal susceptibility data is well fitted by Curie–Weiss expression [$\chi_M = C/(T-\theta)$ with $C = 2.924$ emu K mol^{-1}, $\theta = 25.5$ K] (figure 4), which consolidates the presence of overall ferromagnetic coupling within copper centers. In addition, a sudden decline of $\chi_M T$ below 25 K may be attributed to weak intermolecular interactions and/or antiferromagnetic interactions [11, 27].

In view of the structure and connection motif of coppers in **1**, the overall ferromagnetic exchange interactions occur in the belt-like $\{Cu_6\}$ cluster in the sandwich belt constructed from Cu1, Cu2, Cu3, Cu1A, Cu2A, and Cu3A cores. Similar dominant ferromagnetic coupling interactions have been reported previously in $[Cu(en)_2]_2[Cu(deta)(H_2O)]_2[Cu_6(en)_2(H_2O)_2(B\text{-}\alpha GeW_9O_{34})_2]\cdot 6H_2O$ [11] and $\{[Cu(enMe)_2(H_2O)]_2[Cu_6(enMe)_2(B\text{-}\alpha\text{-}SiW_9O_{34})_2]\}\cdot 4H_2O$ [27]. Previous research suggests that the nature and strength of the magnetic exchange interactions are mainly affected by Cu–O–Cu bond angles. The classical viewpoint on the relationship between the

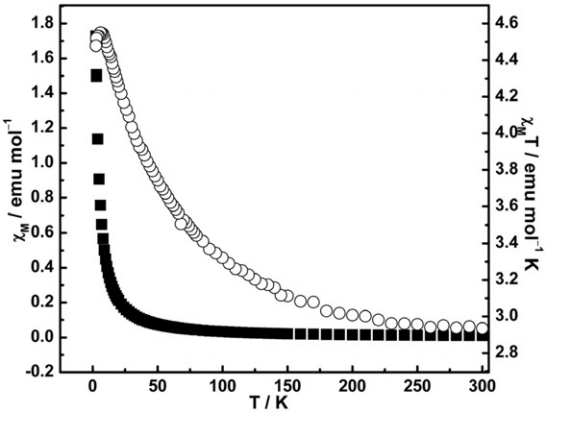

Figure 3. Temperature dependence of the molar magnetic susceptibility χ_M (■) and the $\chi_M T$ (○) product for **1** between 2 K and 300 K.

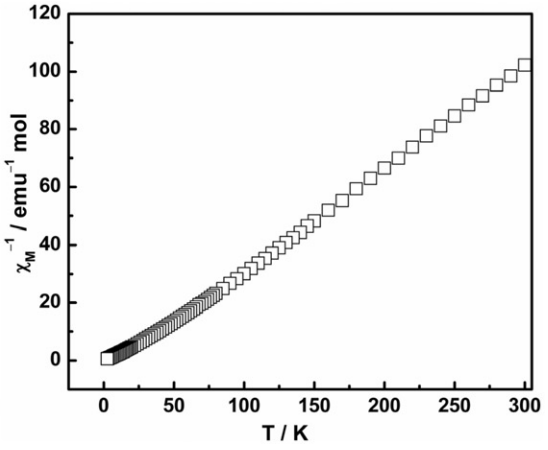

Figure 4. Temperature evolution of the inverse magnetic susceptibility χ_M^{-1} for **1** between 2 K and 300 K.

magnetic coupling constants and Cu–O–Cu bond angles illustrate that the coupling is antiferromagnetic for angles higher than 98° whereas it is ferromagnetic for those lower than 98° [39–41]. Although the Cu–O–Cu bond angles in **1** are 78.3(5)–100.0(4)°, the number of Cu–O–Cu bond angles lower than 98° are more than the ones higher than 98°. Therefore, the overall ferromagnetic coupling within Cu centers should be expected and the continuous increase in $\chi_M T$ on decreasing temperature confirms the point before 6 K. Ferromagnetic exchange interactions of multi-copper substituted POMs have been already observed in previous studies [10, 25, 42]. For example, the ferromagnetic hexa-Cu sandwiched POM polyoxoanion $[(CuCl)_6(AsW_9O_{33})_2]^{12-}$ has been reported by Yamase *et al.* [25]. The predominant ferromagnetic exchange interactions in octa-Cu^{II} substituted POMs $[Cu(H_2O)_2]H_2[Cu_8(dap)_4(H_2O)_2(B\text{-}\alpha XW_9O_{34})_2]$ ($X = Si^{IV}$, Ge^{IV}) [10] and $H_4[Cu_8(dap)_4(H_2O)_2(B\text{-}\alpha\text{-}GeW_9O_{34})_2]\cdot 13H_2O$ have been reported by Zhao *et al.* [42].

4. Conclusion

A coplanar-shaped hexa-Cu^{II} cluster sandwiched AT, which contains the largest number known of paramagnetic TMs of all sandwiched AT, has been hydrothermally synthesized and structurally characterized. The preparation provides opportunities and guidance in designing and creating multi-dimensional hybrid POM materials by structural transition of lacunary AT. The synthesis of **1** not only enriches the diversity of sandwich-type TMSPs chemistry, but also shows that hydrothermal technique offers an effective way for making high-nuclearity TMSPs based on lacunary polyoxoanions. Further work in this area will focus on making other high-nuclear metal cluster aggregations. We believe that much more inorganic–inorganic high-nuclear TMSPs will be investigated in due time; pertinent work is under way in our laboratory.

Supplementary material

CCDC 851928 for **1** contains the supplementary crystallographic data for this article. These data can be obtained free of charge from The Cambridge Crystallographic Data Centre *via* www.ccdc.cam.ac.uk/data_request/cif.

Acknowledgments

This work was financially supported by the Natural Science Foundation of China, Special Research Fund for the Doctoral Program of Higher Education, Innovation Scientists and Technicians Troop Construction Projects of Henan Province, and Natural Science Foundation of Henan Province.

References

[1] M.T. Pope. *Heteropoly and Isopoly Oxometalates*, Springer-Verlag, Berlin (1983).
[2] M.T. Pope, A. Muller (Eds). In *Polyoxometalate Chemistry: From Topology via Self-Assembly to Applications*, Kluwer, Dordrecht, The Netherlands (2001).
[3] J.J. Borrás-Almenar, E. Coronado, A. Müller, M.T. Pope (Eds). In *Polyoxometalate Molecular Science*, Kluwer, Dordrecht, The Netherlands (2003).
[4] T. Yamase. *Chem. Rev.*, **98**, 307 (1998).
[5] C.L. Hill, C.M. Prosser-McCartha. *Coord. Chem. Rev.*, **143**, 407 (1995).
[6] S.Z. Li, J.W. Zhao, P.T. Ma, J. Du, J.Y. Niu, J.P. Wang. *Inorg. Chem.*, **48**, 9819 (2009).
[7] Z.H. Zhang, S. Yao, Y.G. Li, E.B. Wang. *J. Coord. Chem.*, **62**, 1415 (2009).
[8] J.W. Zhao, H.P. Jia, J. Zhang, S.T. Zheng, G.Y. Yang. *Chem. – Eur. J.*, **13**, 10030 (2007).
[9] Y.L. Xu, B.B. Zhou, Z.H. Su, K. Yu, J. Wu. *J. Coord. Chem.*, **64**, 3670 (2011).
[10] J.W. Zhao, C.M. Wang, J. Zhang, S.T. Zheng, G.Y. Yang. *Chem. – Eur. J.*, **14**, 9223 (2008).
[11] J.W. Zhao, S.T. Zheng, Z.H. Li, G.Y. Yang. *Dalton Trans.*, **38**, 1300 (2009).
[12] M.A. Aldamen, S.F. Haddad. *J. Coord. Chem.*, **64**, 4224 (2011).
[13] H. Liu, C. Qin, Y.G. Wei, L. Xu, G.G. Gao, F.Y. Li, X.S. Qu. *Inorg. Chem.*, **47**, 4166 (2008).
[14] Y.H. Liu, P.T. Ma, J.P. Wang. *J. Coord. Chem.*, **61**, 936 (2008).
[15] P.T. Ma, Y. Wang, H.N. Chen, J.P. Wang, J.Y. Niu. *J. Coord. Chem.*, **64**, 2497 (2011).
[16] R. Khoshnavazi, S. Gholamyan. *J. Coord. Chem.*, **63**, 3365 (2010).
[17] U. Kortz, S. Isber, M.H. Dickman, D. Ravot. *Inorg. Chem.*, **39**, 2915 (2000).
[18] P. Mialane, J. Marrot, E. Rivière, J. Nebout, G. Hervé. *Inorg. Chem.*, **40**, 44 (2001).
[19] F. Hussain, M. Reicke, U. Kortz. *Eur. J. Inorg. Chem.*, 2733 (2004).
[20] U. Kortz, M.G. Savelieff, B.S. Bassil, B. Keita, L. Nadjo. *Inorg. Chem.*, **41**, 783 (2002).
[21] Z. Luo, P. Kögerler, R. Cao, C.L. Hill. *Inorg. Chem.*, **48**, 7812 (2009).
[22] L.H. Bi, U. Kortz. *Inorg. Chem.*, **43**, 7961 (2004).
[23] Z. Luo, P. Kögerler, R. Cao, C.L. Hill. *Polyhedron*, **28**, 215 (2009).
[24] L.H. Bi, U. Kortz, S. Nellutla, A.C. Stowe, J.V. Tol, N.S. Dalal, B. Keita, L. Nadjo. *Inorg. Chem.*, **44**, 896 (2006).
[25] T. Yamase, K. Fukaya, H. Nojiri, Y. Ohshima. *Inorg. Chem.*, **45**, 7698 (2006).
[26] Z.M. Zhang, Y.G. Li, E.B. Wang, X.L. Wang, C. Qin, H.Y. An. *Inorg. Chem.*, **45**, 4313 (2006).
[27] S.T. Zheng, D.Q. Yuan, J. Zhang, G.Y. Yang. *Inorg. Chem.*, **46**, 4569 (2007).
[28] J.P. Wang, J. Du, J.Y. Niu. *CrystEngComm*, **10**, 972 (2008).
[29] J.Y. Niu, X. Ma, J.W. Zhao, P.T. Ma, C. Zhang, J.P. Wang. *CrystEngComm*, **13**, 4834 (2011).
[30] C. Tourné, A. Revel, G. Tourné, M.C.R. Vendrell. *Acad. Soc. Paris, Ser. C*, 1973, t277, 643. IR (KBr disk): 931 (m), 903 (s), 781 (s), 725 cm^{-1} (s).
[31] G.M. Sheldrick. *SHEXTL-97, Programs for Crystal Structure Refinements*, University of Göttingen, Germany (1997).
[32] L.J. Chen, Y.H. Fan, J.W. Zhao, P.T. Ma, D.Y. Shi, J.P. Wang, J.Y. Niu. *J. Coord. Chem.*, **63**, 2042 (2010).
[33] Q.X. Han, P.T. Ma, J.W. Zhao, J.P. Wang, J.Y. Niu. *Inorg. Chem. Commun.*, **14**, 767 (2011).

[34] J.W. Zhao, D.Y. Shi, L.J. Chen, P.T. Ma, J.P. Wang, J.Y. Niu. *CrystEngComm*, **13**, 3462 (2011).
[35] C.Y. Sun, Y.G. Li, E.B. Wang, D.R. Xiao, H.Y. An, L. Xu. *Inorg. Chem.*, **46**, 1563 (2007).
[36] Q.X. Han, P.T. Ma, J.W. Zhao, Z.L. Wang, W.H. Yang, P.H. Guo, J.P. Wang, J.Y. Niu. *Cryst. Growth Des.*, **11**, 436 (2011).
[37] A. Dolbecq, J.D. Compain, P. Mialane, J. Marrot, E. Rivière, F. Sécheresse. *Inorg. Chem.*, **47**, 3371 (2008).
[38] B. Li, J.W. Zhao, S.T. Zheng, G.Y. Yang. *Inorg. Chem.*, **48**, 8294 (2009).
[39] E. Ruiz, P. Alemany, S. Alvarez, J. Cano. *J. Am. Chem. Soc.*, **119**, 1297 (1997).
[40] G. Aromí, J. Ribas, P. Gamez, O. Roubeau, H. Kooijman, A.L. Spek, S. Teat, E. MacLean, H. Stoeckli-Evans, J. Reedijk. *Chem. – Eur. J.*, **10**, 6476 (2004).
[41] M.P. Shores, B.M. Bartlett, D.G. Nocera. *J. Am. Chem. Soc.*, **127**, 17986 (2005).
[42] J.W. Zhao, J. Zhang, S.T. Zheng, G.Y. Yang. *Chem. Commun.*, 570 (2008).